

# Gas7 knockout affects PINK1 expression and mitochondrial dynamics in mouse cortical neurons

Jagannatham Naidu Bhupana<sup>1,2</sup> | Bo-Tsang Huang<sup>2</sup> | Gunn-Guang Liou<sup>2</sup> | Marcus J. Calkins<sup>3</sup> | Sue Lin-Chao<sup>1,2</sup>

<sup>1</sup>Molecular Cell Biology, Taiwan International Graduate Program, Institute of Molecular Biology, Academia Sinica and Graduate Institute of Life Sciences, National Defense Medical Center, Taipei, Taiwan

<sup>2</sup>Institute of Molecular Biology, Academia Sinica, Taipei, Taiwan

<sup>3</sup>Institute of Cellular and Organismic Biology, Academia Sinica, Taipei, Taiwan

## Correspondence

Sue Lin-Chao, Institute of Molecular Biology, Academia Sinica, Taipei 11529, Taiwan.

Email: mbsue@gate.sinica.edu.tw

## Funding information

Institute of Molecular Biology, Academia Sinica, Grant/Award Number: 2323

## Abstract

Dynamic fission and fusion events regulate mitochondrial shape, distribution, and rejuvenation, and proper control of these processes is essential for neuronal homeostasis. Here, we report that *Gas7*, a known cytoskeleton regulator, controls mitochondrial dynamics within neurons of the central nervous system. In this study, we generated an improved *Gas7*-knockout mouse and evaluated its mitochondrial phenotype. We first identified *Gas7* in mitochondrial fractions from wild-type brain tissue, and observed *Gas7* colocalization with mitochondria in primary cortical neurons. In *Gas7*-deficient brain tissue and neuronal cultures mitochondria were elongated with perinuclear clustering. These morphological abnormalities were associated with increased levels mitochondrial fusion proteins and increased PKA-dependent phosphorylation of Drp-1 in brain tissues, suggesting an imbalance of mitochondrial fusion and fission. Moreover, expression of mitochondrial quality control kinase, PINK1, and PINK1-specific phosphorylation of Mfn-2 (S442), Parkin (S65), and ubiquitin (S65) were all reduced in the knockout cells. Ectopic expression of *Gas7* restored mitochondrial morphology and distribution, as well as PINK1 expression in *Gas7*-null cortical neurons. Collectively, our results introduce a novel role of mouse *Gas7* in determining the dynamics, morphology, and intracellular distribution of neuronal mitochondria, which are expected to be required for normal neuronal function.

## KEYWORDS

Drp-1, mitochondria, Mitofusin-2, Parkin, PINK1

## 1 | INTRODUCTION

The gene for growth arrest-specific 7 (*Gas7*) was discovered using a retrovirus-based gene trapping strategy in growth-arrested NIH3T3 fibroblasts.<sup>1,2</sup> *Gas7* protein belongs to the

F-BAR (FCH-Bin-Amphiphysin-Rvs) domain protein family,<sup>3</sup> which comprises a variety of regulatory proteins that induce membrane deformation.<sup>4,5</sup> Mouse *Gas7* has been shown to play a role in actin polymerization<sup>6</sup> and functions in neurite outgrowth in various cultured cells, including embryonic primary cultured

**Abbreviations:** CDK5, cyclin-dependent kinase 5; CREB, cyclic AMP response element-binding protein; Drp-1, dynamin-related protein 1; F-BAR, Fes/CIP4 homology Bin-Amphiphysin-Rvs; *Gas7*, growth arrest-specific gene 7; Mfn-1, Mitofusin-1; Mfn-2, Mitofusin-2; Opa-1, optic atrophy type 1; Pdh, pyruvate dehydrogenase; PINK1, PTEN-induced putative kinase; PKA, cyclic AMP-dependent protein kinase A.

This is an open access article under the terms of the Creative Commons Attribution-NonCommercial License, which permits use, distribution and reproduction in any medium, provided the original work is properly cited and is not used for commercial purposes.

© 2020 The Authors.

neurons.<sup>7</sup> The Gas7 protein binds directly with F-actin<sup>6</sup> and its specific interaction with N-WASP induces actin polymerization during neurite outgrowth of hippocampal neurons.<sup>8</sup> Human Gas7 (hGAS7b) is 97% homologous to the murine protein<sup>9</sup> and was identified as a regulator of tubulin polymerization.<sup>10</sup> The binding between hGas7b and microtubule-associated protein Tau stabilizes polymerized microtubules.<sup>10</sup> Because Tau protein level is inversely correlated with hGAS7b level, it has been suggested that hGAS7b may play a role in the Tau-associated pathology of Alzheimer's disease.<sup>10,11</sup> Notably, excess hGAS7b protein was found to directly bind to microtubules, where it interferes with kinesin movement.<sup>12</sup> Thus, the importance of Gas7 in neuronal cytoskeletal structure has been firmly established.

A *Gas7*-deficient/mutant mouse strain was previously generated by homozygous deletion of the chromosomal region encoding exon 6b,<sup>13</sup> however, this genetic modification still allows for the production of an unstable *Gas7* derivative that retains functions similar to the wild-type protein. In aging *Gas7*-mutant mice, neuromuscular junctions exhibit reduced terminal sprouting of neurons, muscle fiber composition abnormalities, and motor activity defects.<sup>13</sup> When a multistep approach was used to dissect the genetics of complex traits for disease phenotypes, *hGAS7b* was identified as a candidate causal gene for abdominal obesity.<sup>14</sup> Interestingly, when transgenic male mice that overexpress human GAS7 are placed on a high-fat diet, the animals exhibit enhanced shared metabolic pathways and transcriptional networks in liver tissue with coincident reductions in fat mass and body weight compared with control mice.<sup>14,15</sup> Notably, native *Gas7* is not expressed in mouse liver tissue,<sup>5</sup> but expression of the *hGAS7b* transgene was detected in liver tissues in transgenic mice.<sup>14</sup> Overall, these studies suggest that in addition to regulating actin and microtubule function, *Gas7* may have other as-yet unidentified functions.

Here, we generated a new line of mice lacking *Gas7*. These *Gas7*-knockout mice are born and appear to develop normally, similar to the previous *Gas7*-mutant mice.<sup>13</sup> However, unlike the *Gas7*-mutant mice, *Gas7* knockouts exhibit altered mitochondrial dynamics and elongated mitochondria in neurons. Ectopic expression of *Gas7* in primary cortical neurons rescued this mitochondrial phenotype. Further analysis of brain tissue revealed changes in the protein levels of key homeostatic regulators of mitochondrial dynamics, mitophagy, and mitochondrial physiology in *Gas7*-knockout mice compared with wild-type mice. Our data introduce a novel role for *Gas7* in maintaining normal fission, fusion, and transport of healthy mitochondria.

## 2 | MATERIALS AND METHODS

### 2.1 | Ethics statement

Mice were handled and housed in accordance with the guidelines for animal care of the National Laboratory

Animal Center (NLAC) of Taiwan. All procedures were authorized by the Academia Sinica Institutional Animal Care and Utilization Committee (IACUC), protocol #RMIIMBCS2009040.

### 2.2 | Generation of *gas7*-knockout mice and breeding

The *gas7*-knockout mice were generated from embryonic stem (ES) cells of the 129 mouse strain by targeting exons 5 to 11 of *Gas7* with pGK-neo (neomycin gene)<sup>16</sup> using two vectors with loxp sites by subcloning. Electroporation, selection, and screening of ES cells were conducted as reported previously.<sup>17,18</sup> Selected ES clones were expanded for blastocyst injection into C57BL/6 mice to produce chimeric mice. Male chimeras with a high proportion of agouti coat color were bred with C57BL/6 females for germline transmission of the targeted allele. The agouti heterozygous offspring were crossed to generate homozygous knockout mice that were then backcrossed for at least six generations with C57BL/6 mice to obtain a 95% C57BL/6 background in *gas7*-knockout mice. Genotypes were confirmed by single nucleotide polymorphism (SNP) genotyping by the National Center for Genome Medicine (located at the Institute of Biomedical Sciences, Academia Sinica). Genotype analysis by PCR was performed on mouse tail genomic DNA using primers P1 5'-GTT CAG CCT TCC TCC ACT TGC-3' and P2 5'-AGT GAA TGG GAA ACT GAC AGA GG-3' to amplify ~492 base pairs in wild-type, and P3 5'-ATA GCG GCC GCA GCC ATC ATG ACA GAG AA-3' and P4 5'-ATA GTC GAC GTT AAG GAC ACA CTG GTT CT-3' to amplify ~625 base pairs in heterozygote mice and in *Gas7*-knockout mice.

### 2.3 | Western blot analysis

After lysis of cerebrum tissue and centrifugation, the supernatant was transferred to a fresh tube and loaded onto an SDS-polyacrylamide gel, and then transferred to a nitrocellulose membrane (Millipore, IPVH00010, and Billerica MA). The membrane was blocked in TBS buffer containing 20 mM Tris pH 7.6, 137 mM NaCl, and 5% nonfat dry milk or BSA for 1 hour and then incubated overnight at 4°C in TBS containing respective antibodies. The membrane was washed three times for 10 minutes each in TBST (TBS + 0.05% Tween 20) and then incubated with secondary antibody (IgG conjugated with horseradish peroxidase; GE Healthcare, Buckinghamshire, NA931V, NA934V, UK). After 60 minutes, blots were washed three times for 30 minutes each with TBST and visualized by ECL (GE Healthcare, RPN2106, and Buckinghamshire, UK).

## 2.4 | Antibodies used in this study

The following antibodies were purchased from commercial sources:  $\alpha$ -Parkin polyclonal antibody (Cell Signaling, 2132S),  $\alpha$ -phospho-Parkin (S65) (Abcam, ab154995),  $\alpha$ -ubiquitin monoclonal antibody (Santa Cruz Biotechnology, SC-8017),  $\alpha$ -phospho-ubiquitin (S65) (Boston Biochem, 13568315A),  $\alpha$ -actin (Santa Cruz Biotechnology, SC-47778),  $\alpha$ -GAPDH antibody (Chemicon, AB2302),  $\alpha$ -SDHA antibody (Abcam, ab14715), and polyclonal antibodies for  $\alpha$ -GM-130 (Abcam, ab40881-100),  $\alpha$ -PINK1 (Novus Biologicals, BC 100-494),  $\alpha$ -mitofusin-2 (Sigma-Aldrich, HPA030554),  $\alpha$ -phospho-mitofusin-2(S442) (Millipore, ABC963),  $\alpha$ -mitofusin-1 (Abcam, ab57602),  $\alpha$ -FIS1 (Sigma-Aldrich, HPA017430),  $\alpha$ -Drp-1 (Abcam, ab56788),  $\alpha$ -phospho-Drp-1(S637) (Cell Signaling, 6319S),  $\alpha$ -phospho-Drp-1(S616) (Cell Signaling, 4494T), and  $\alpha$ -phospho-CREB (Cell Signaling, 919L).  $\alpha$ -Pdh (Abcam, ab11034),  $\alpha$ -phospho-Pdh (S293) (Sigma-Aldrich, ABS204),  $\alpha$ -CDK-5 (Abcam, ab151233), and  $\alpha$ -Gas7 antibody were prepared from rabbits immunized with His tag-fused mouse full-length Gas7, as described previously.<sup>7</sup> The anti-Gas7 antibody detects Gas7 and the hGAS7b form.<sup>10</sup>

## 2.5 | Cortical neuron culture and preparation of cell lysates

For preparation of primary cortical neurons, we maintained isolated cortical tissue from C57BL/6 mice at embryonic day 16 in Hanks' balanced salt buffer with 1% glucose, 100 ng/ml streptomycin, and 100 U/ml penicillin. The tissues were digested with 0.05% trypsin plus 1 mM EDTA for 3 minutes and triturated through a flame-polished Pasteur pipette to disrupt cell-cell adhesions. Dispersed cells were centrifuged and cultured in Neurobasal Medium (Invitrogen) with B27 complex and 1 mM L-glutamine. The primary neurons were seeded on 12-well ( $1 \times 10^5$  cells per well) plates or a 3.5 cm dish ( $3 \times 10^5$  cells per dish) coated with poly-L-lysine. The cells were cultured in vitro for 7 days. Before tissue lysate preparation, the cerebrum tissue was rinsed twice with ice-cold phosphate-buffered saline and solubilized in RIPA buffer (150 mM NaCl, 50 mM Tris pH 7.9, and 0.5% DOC [sodium deoxycholate] containing 1.0% NP 40 and 0.1% SDS). Lysates from mouse cerebrums were prepared from 60-day-old wild-type, heterozygous, and knockout genotypes of Gas7 mice after homogenization using a Tissue Lyser (Qiagen, 85210) with RIPA buffer. Supernatants were collected after centrifugation at  $14\,000 \times g$  for 15 minutes at 4°C. Protein concentrations were determined using a detergent-compatible protein assay kit (Bio-Rad, 500-0006).

## 2.6 | Immunofluorescence staining of primary cortical neurons

Cortical neurons were isolated from embryonic day 16.5 C57BL/6 mice as previously described.<sup>13</sup> Following isolation of neurons from mouse cortex, neurons were fixed with 4% PFA (Electron Microscopy Sciences, 15710), and then blocked in PBS containing 10% normal goat serum, 2% BSA, and 0.2% Triton X-100 (PBST). Primary antibodies were prepared in 10% normal goat serum and 1% BSA in PBST. Samples were incubated with primary antibody at 4°C overnight, washed in PBS three times for 10 minutes each, and stained with secondary antibody conjugated to FITC and Cy3 (Invitrogen). Images of cross-sections were captured with a confocal LSM 510 system (Carl Zeiss Microimage). Mitochondria and Gas7 colocalization was detected by using FITC conjugation for mitochondria and Cy3 conjugation for Gas7, respectively. Images of cortical neurons were captured with a confocal LSM780 system (Carl Zeiss Microimage).

## 2.7 | Fractionation and mitochondrial and cytosolic isolations

After dissection of the cerebrum from wild-type mice, cerebrums were washed with washing buffer, homogenized with a motorized Kontes Microtube Pellet Pestle Rod in isolation buffer, and centrifuged at  $1000 \times g$  for 10 minutes. Pellets containing the nuclear-enriched fractions were saved and the supernatants were used for isolation of different organelles. The homogenized solution was subjected to 15%-35% sucrose gradient ultracentrifugation. Centrifugation was performed at 4°C for 4 hours at 37 200 rpm using a SW40Ti (Beckman) rotor following gradient formation. After centrifugation, 17 fractions were collected and subjected to Western blot and probed with different antibodies for detection of specific proteins. We used antibodies against the subcellular marker proteins SDHA, GM130, and actin to tag mitochondria, Golgi complex, and cytosol, respectively, in the sucrose density gradient fractions. For isolation of mitochondria and cytosol from mouse cerebrum tissue, cerebrums were dissected from wild-type mice. After dissection, mitochondrial and cytosolic fractions were isolated from cerebrums using a Mitochondria Isolation Kit for Tissue (Abcam, ab110168) according to the manufacturer's instructions. Briefly, cerebrums were washed with washing buffer, homogenized with a motorized Kontes Microtube Pellet Pestle Rod in isolation buffer, and centrifuged at  $1000 \times g$  for 10 minutes. Pellets containing the nuclear-enriched fractions were saved, and supernatants were centrifuged again at  $12\,000 \times g$  for 15 minutes. The supernatants containing the cytosolic fractions were saved and the pellets

containing the mitochondrial fractions were washed twice with isolation buffer and resuspended in isolation buffer combined with complete protein inhibitor cocktail (Roche Applied Bioscience). Following centrifugation, the pellets were enriched with mitochondria, whereas the supernatant maintained the cytosolic fraction. Protein concentrations were determined using a detergent-compatible protein assay kit (Bio-Rad, 500-0006). Equal protein was loaded from each fraction and Western blotting was performed with antibodies against SDHA for the mitochondrial fraction and GAPDH for the cytosolic fraction.

## 2.8 | Electron microscopy analysis of mitochondria from mouse cortex

We performed ultrastructural examination of osmium tetroxide/uranyl acetate-stained mouse cortex sections using a Tecnai G2 Spirit TWIN system (FEI Company). Mouse cortex was isolated from wild-type and *gas7*-knockout mice and, after isolation, cortical tissues were washed thoroughly with filtered phosphate buffered saline (PBS) pH 7.4, post-fixed for 1 hour with 1% osmium tetroxide in PBS, rinsed with PBS, and dehydrated in 50% and 70% ethanol baths. A 2% uranyl acetate in 70% ethanol solution was applied for contrast (1 hour at 25°C in the dark), followed by two rinses in 70% ethanol (5 minutes each). Dehydration in ethanol was completed with two steps of 5 minutes in 95% and 100% ethanol baths. Then, 100% propylene oxide (Electron Microscope Sciences) was applied to the samples (two baths of 10 minutes each). Samples were then placed gradually in a 1:1 mixture of propylene oxide and Epon resin (25.9% Embed 812, 15.5% Araldite 502, 55.9% DDSA, and 2.7% BDMA; all resin components from Electron Microscope Sciences) for 1 hour at 25°C, then in a 1:2 mixture of propylene oxide-Epon resin (1 hour at 25°C), and finally transferred into pure Epon resin and kept overnight at 25°C. The following day, the samples were placed in freshly prepared resin for an additional hour at 25°C and finally allowed to polymerize in an oven at 70°C for a minimum of 4 days. Ultrathin sections were obtained using a Leica EM UC6 ultra microtome (Leica Microsystems) before being mounted on formvar-coated copper grids and observed and photographed using an Hitachi transmission electron microscope, model H7650 (Hitachi, Japan), equipped with a Hamamatsu ORCA-HR digital camera. Mitochondria were visually marked and analyzed. Mitochondria aspect ratio (the ratio of length/width) was measured and quantified using Metamorph software. Elongated mitochondria were quantified from a mitochondrial population of  $N = 823$  wild-type and  $N = 1235$  *gas7*-knockout mouse cortical sections. Statistical significance was assessed by Student's *t* test;  $*P < .001$ .

## 2.9 | Metabolic phenotyping

Metabolic rates (food and water intake, locomotor activity,  $VO_2$  consumption, and  $VCO_2$  production)<sup>19</sup> were measured using a four-cage Promethion-C continuous, parallel metabolic phenotyping system (Sable Systems International [SSI]) for six wild-type and six *gas7*-knockout male mice (36 weeks old). This system imposes minimal stress due to handling or other disruptive influences because it uses live-in cages of ~4L STP internal volume that are transferred from the housing colony to the testing room for studies. Air was pulled from the cages at a controlled mass flow rate of 2L/min STP. This yielded a time constant of ~4 minutes. The flow from each cage was sampled by a gas analysis chain consisting of a water vapor analyzer, a  $CO_2$  analyzer, an  $O_2$  analyzer, a barometric pressure sensor, and a subsampling flow control system, all integrated into one gas analysis system (GA3m4: SSI) per bank of four cages. Gas flow for each bank was generated by a FR-4b mass flow-controlled pull flow generator (SSI). The calorimetric room had a fluorescent light source controlled by a timer set to a 12:12 hours light:dark cycle. Monitoring was performed for 5 days after mice had acclimatized to cages for 2 days. The respiration quotient (RQ) was calculated as the ratio of  $VCO_2/VO_2$ .<sup>20</sup> The system acquired data on fractional  $O_2$  and  $CO_2$  concentrations, running wheel speed, water vapor pressure (WVP), barometric pressure (BP), ambient temperature and light levels, flow rates, food and water dispenser masses (to 1 mg), body masses (to 1 mg via a weighed enrichment habitat), running wheel revolutions, and X, Y and Z locations together with beam breaks. Measurements were acquired at a sample rate of 1 sample/sec for all sensors and cages simultaneously via an error-correcting control area network (CAN). The provision for exercise increased variability in Energy Expenditure (EE)<sup>21</sup> and RQ for a total of  $N = 108$  measurements of six wild-type and six *gas7*-knockout male mice for all parameters measured in this study.

## 2.10 | Analysis of mitochondrial morphology in cortical neurons (Micro-P)

Neuronal cells were isolated from wild-type and *gas7*-knockout mice cortex of embryonic day 16.5 embryos and cultured for 7 days as described above. The neuronal cells were then stained with anti-SDHA as a mitochondrial marker and cell images were taken by confocal LSM780 system (Carl Zeiss Microimage). Wild-type, *gas7* KO, and GFP-Gas7 cortical neurons ( $N = 5$ ) were then analyzed using the Micro-P software.<sup>22</sup> That software measures individual mitochondria (by detecting SDHA antibody signal) according to morphological, skeletal, and textural features, and sorts them into six types.<sup>22</sup> Small fragmented mitochondria with a pixel area  $<20$  were categorized as type 1. Large fragmented mitochondria with a

length/width ratio  $<3$  were type 2. Of the remaining mitochondria, curved, branched, or circular tubular mitochondria with a length/width ratio 2 were grouped as type 3, curved tubular mitochondria with a length/width ratio  $>2$  were designated as type 4, horseshoe/donut/network tubular mitochondria with a length/width ratio  $<3$  were type 5, and network tubular mitochondria with a length/width ratio  $>3$  were designated as type 6. We employed the Micro-P software for mitochondrial distribution and heterogeneity analysis of wild-type, *gas7*-knockout, and GFP-*Gas7* cortical neurons ( $N = 5$ ).

### 3 | RESULTS

#### 3.1 | Generation and validation of *Gas7*-knockout mice

*Gas7*-knockout mice were generated from embryonic stem cells of 129 mice by targeting exons 5 to 11 of *Gas7* with pGK-neo.<sup>16</sup> As shown in Figure 1A, upon deletion of exon 5 to 11, a frameshift and premature stop codon were generated in exon 12. Genotyping was performed using genomic DNA from wild-type and *Gas7*-knockout mouse tails. The wild-type allele was PCR amplified using primers P1 and P2, producing a 492 bp

product; meanwhile, the mutant allele was amplified by P3 and P4, producing a 625 bp product (Figure 1A). As shown in Figure 1B, wild-type mice were identified by a single band at 492 bp, heterozygous mice had bands at 492 and 625 bp, and the homozygous *Gas7*-knockout mice were identified by only a 625 bp band (Figure 1B; lane 1/WT, lane 2/HT, and lane 3/KO). Western blot analysis was then performed using an antibody against *Gas7* protein and brain lysates from WT, HT, and KO mice (Figure 1C). We detected about twice as much *Gas7* protein in the wild type as the heterozygous mice (Figure 1C, comparing lane 1 with lane 2). As expected, *Gas7* protein was not detected in the *Gas7*-knockout brain lysate (Figure 1C, lane 3). No obvious differences were observed in the expression of antitubulin from the same brain lysates (Figure 1C lower panel). Thus, deletion of exons 4 to 11 of the *Gas7* gene resulted in a complete lack of detectable *Gas7* protein in the homozygous knockout, suggesting that we successfully produced true *Gas7*-knockout mice.

#### 3.2 | *Gas7* associates with mitochondria in mouse cortical neurons

To determine the subcellular distribution of *Gas7*, we performed ultracentrifugation of mouse brain lysate on a sucrose

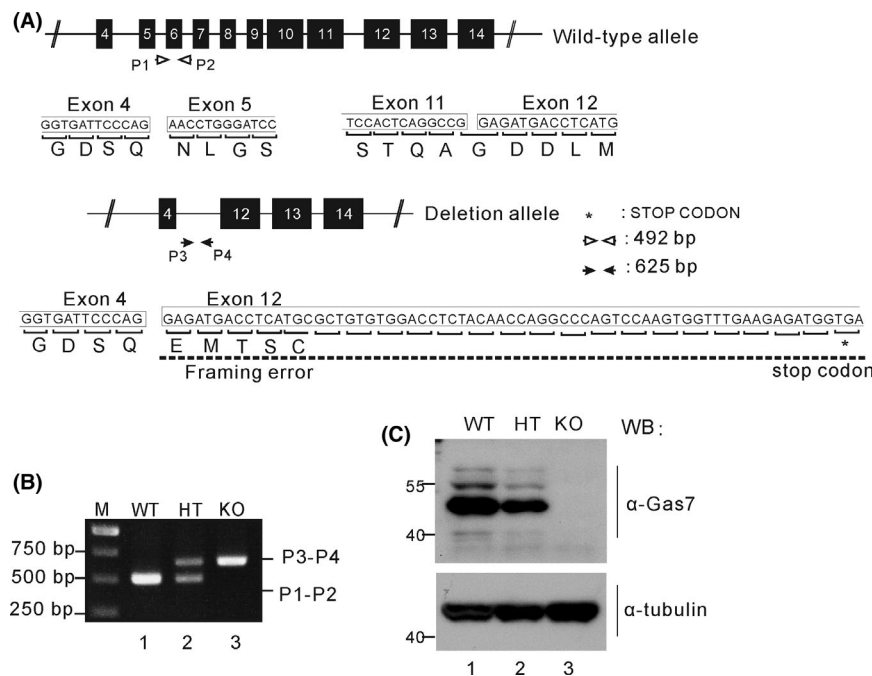


**FIGURE 1** Generation, genotyping, and characterization of *gas7*-knockout mice. A, The structure of the *Gas7* wild-type and deletion (knockout) allele. For *Gas7* gene targeting, we excised the region from exons 5 to 11 of *Gas7* genomic DNA and generated a framework error and stop codon in exon 12 that prevented the alternative splicing responsible for forming truncated *Gas7*. The *Gas7* wild-type and deletion allele were verified by two primer pairs, P1-P2 and P3-P4. The predicted PCR product length of the P1-P2 primers is 492 base pairs (bp) and for the P3-P4 pair it is 625 bp. White arrows indicate the P1 and P2 primers; black arrowheads indicate the P3 and P4 primers. B, Genotype analysis by PCR was performed on mouse tail genomic DNA. PCR products amplified a ~492 bp fragment in wild-type and a ~625 bp fragment in knockout mice, and both fragments were found in the heterozygotes. M indicates a 1 kb DNA ladder (Fermentas). C, Western blot analysis. Total brain lysates from wild-type (WT), *gas7* heterozygous (HT), and *gas7*-knockout (KO) mice were electrophoresed by 10% SDS-PAGE. After blotting, the membranes were probed with *Gas7* antibody to show that *Gas7* protein exists in WT and *gas7* HT but not in *gas7* KO mice

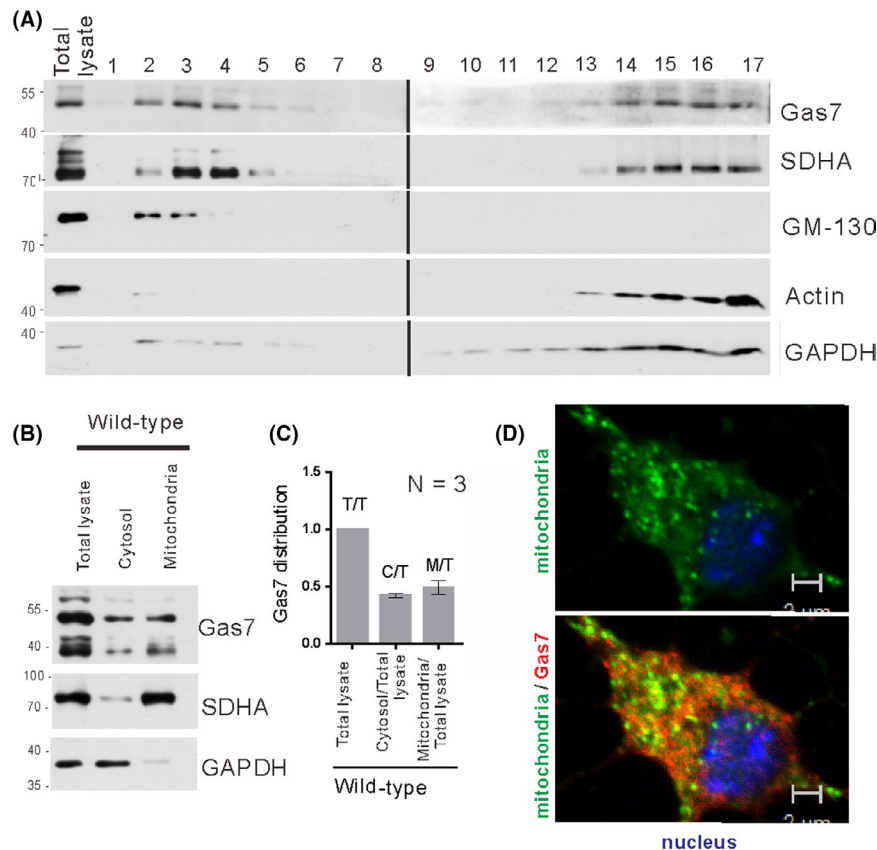


**FIGURE 2** Gas7 detection and localization with mitochondria. A, Sucrose gradient fractionation of mouse cerebrum homogenate. Homogenized solutions were subjected to ultracentrifugation in 15%-35% sucrose gradients. Fractions were then resolved by SDS-PAGE and immunoblotted with an antibody against Gas7. Gas7 was detected in fractions 2-4 and 14-17, SDHA in fractions 3 and 4 and 14-17, GM-130 in fractions 2 and 3, and actin and Gapdh in fractions 14-17. B, Immunoblots of Gas7, SDHA, and GAPDH of isolated mitochondrial, cytosolic, and total lysate fractions from WT cerebrum showing that Gas7 is distributed in cytosol and mitochondrial fractions of WT mice. SDHA and GAPDH were used as markers for mitochondrial and cytosolic fractions, respectively. C, Quantification analysis of Gas7 showing that Gas7 is detected in both cytosol and mitochondria fractions. Gas7 detected in the abovementioned fractions was normalized with markers for mitochondrial (SDHA) and cytosolic (GAPDH) fractions, respectively. D, Immunofluorescence analysis of Gas7 and mitochondria colocalization in primary cortical neurons. Top panel shows Gas7 (red) labeled with Gas7 polyclonal antibodies and mitochondria (green) are labeled with SDHA antibody. Bottom panel shows the colocalization (yellow) of Gas7 and mitochondria in a merged image

density gradient, followed by Western blotting with anti-Gas7, anti-SDHA (mitochondria marker), anti-GM130 (Golgi marker), and anti-Actin or anti-GAPDH (cytoplasmic markers) antibodies. As shown in Figure 2A, Gas7 was predominantly detected in fractions 2, 3, and 4, with fractions 3 and 4 being highly enriched in mitochondrial marker and fractions 2 and 3 enriched in Golgi marker. Fractions 13 to 17 contained a cytosol and a mitochondrial mixed fraction, with Gas7 and SDHA both detected. For all samples, the SDHA-specific mitochondrial marker and cytoplasmic GAPDH marker were used both as loading controls and also to monitor the quality of the fraction preparation. The quantitative data normalized to the total brain lysate protein (Figure 2B,C) show a similar distribution of Gas7 in the cytosol and mitochondrial fractions. As shown in Figure 2D, we also validated the association of Gas7 with mitochondria in primary cortical neurons by immunostaining. The bottom panel of Figure 2D shows the colocalized signal (yellow) of mitochondria (SDHA, green, top panel) and the

Gas7 (Gas7, red, bottom panel). Together, the immunoblotting and immunostaining results suggest that Gas7 associates with mitochondria in mouse cortical neurons.

### 3.3 | Brain tissue mitochondria are elongated in Gas7-knockout mice

Based on the colocalization of mitochondria and Gas7 in mouse cortical neurons, we examined the possible function of the protein by comparing the mitochondrial morphology in brain tissue from wild-type and *Gas7*-knockout mice. In sections of cortical brain tissue, more elongated mitochondria were observed in *Gas7*-knockout samples than wild type (Figure 3A). We quantified the mitochondrial aspect ratio (length/width) of wild-type (N = 827) and *Gas7*-knockout (N = 1235) mitochondria in cortical sections (Figure 3B). The average aspect ratio of *Gas7*-knockout mitochondria was 1.75 compared with

the aspect ratio in wild types of 1.59. This difference also supported the notion that mitochondria in *Gas7*-knockout cortex are longer than those in wild-type tissue. *Gas7*-knockout tissue also exhibited a wider range of aspect ratios and more outliers. These results suggest that the absence of *Gas7* may somehow lead to mitochondrial elongation in mouse cortical neurons.

### 3.4 | Mitochondrial morphology is altered in *Gas7*-knockout cortical primary neurons and rescued by ectopic *Gas7* expression

Mitochondria undergo dynamic fission and fusion to regulate mitochondrial shape, distribution, quality, and function.<sup>23,24</sup> Based on our observation of elongated mitochondria in the

cortex of *Gas7*-knockout mice, we further analyzed mitochondrial morphology in primary cortical neurons of wild-type and *Gas7*-knockout mice by well-established methods for cell imaging and a Matlab-based automatic classification (Micro-P).<sup>22</sup> As shown in Figure 4A, the mitochondrial distribution in primary neurons differed between wild-type and *Gas7*-knockout cultures. Mitochondria were heavily concentrated in the cell bodies of *Gas7*-knockout neurons, but were more evenly distributed in wild-type neurons, including substantial distribution into neurites. The Micro-P analysis also showed that the mitochondrial subtypes of the primary cultured neurons of the *Gas7* knockouts differed from wild types (Figure 4Ba). Using 3D Micro-P software to quantify the average distance between all mitochondria and nuclear boundaries in neurons, the results show that the average distance between wild-type mitochondria and nuclear boundaries is more than twice that of *Gas7* knockouts

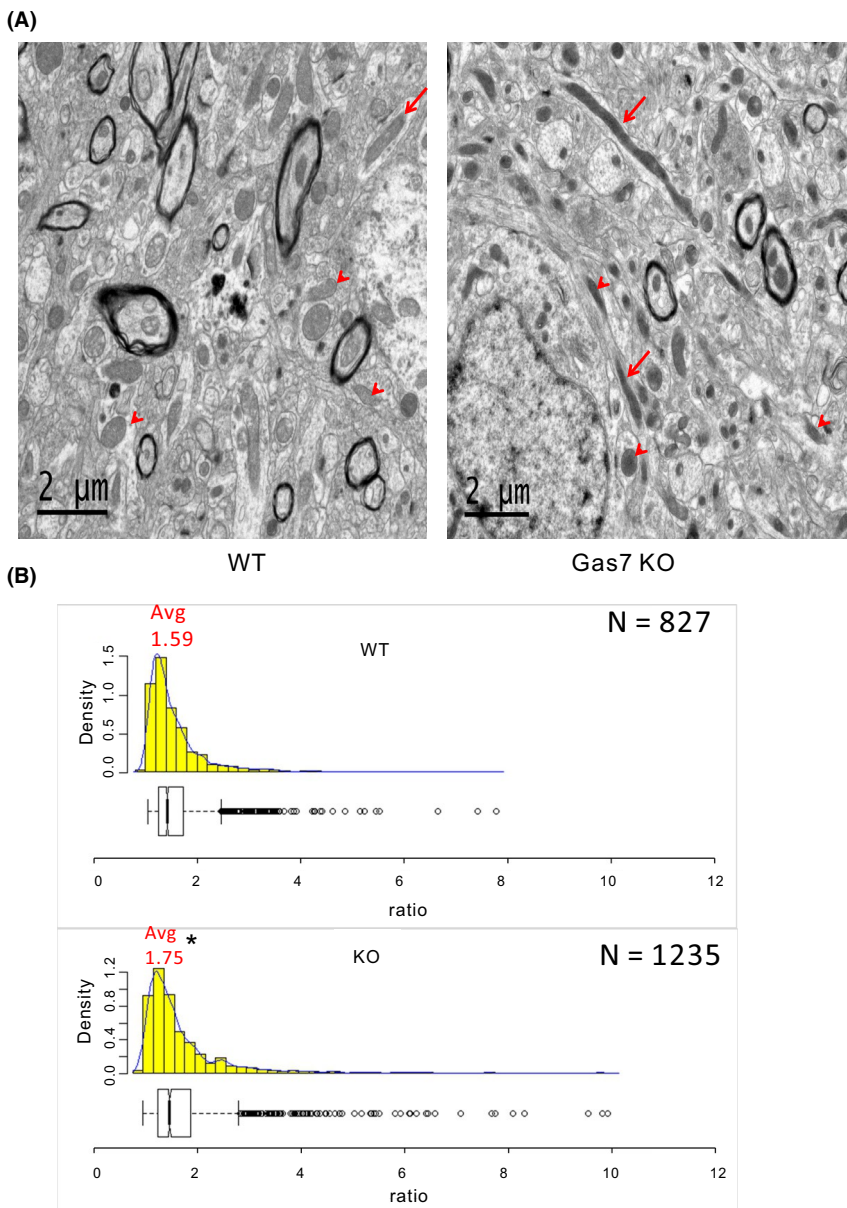


**FIGURE 3** Mitochondrial length increases in *gas7*-knockout mouse brain cortex compared with wild-type mice. A, Wild-type (left panel) and *gas7*-knockout (right panel) mouse cortex showing mitochondria with different aspect ratios (length-to-width ratio). As defined by the box plot in B, outliers are marked with red arrows and nonoutliers are marked with red arrowheads. B, Histogram and box plot of mitochondria aspect ratios from wild-type (left) (N = 823) and *gas7*-knockout (right) cortical sections (N = 1235). \* $P < .001$ . Avg, average. The minimum value of the aspect ratio (length-to-width ratio) of a mitochondrion is 1 when its length equals its width. Bin widths of histograms are equivalent to aspect ratio increments of 0.2. Count represents the number of mitochondria per bin width

(Figure 4Bb, comparing WT with *Gas7*-KO). By overexpressing a *Gas7*-GFP fusion in the knockout primary neurons, the mitochondrial distribution phenotype was largely rescued (Figure 4A,B, comparing *Gas7*-KO vs *Gas7*-KO + *Gas7*-GFP fusion). In addition, Micro-P analysis showed that the mitochondrial subtype populations also changed in *Gas7*-null neurons. As shown in Figure 4C, mitochondrial subtype 1 (small fragmented mitochondria) was predominant in wild-type

cultures, followed by subtypes 3 (curved, branched, or circular tubular mitochondria) and 6 (branched mitochondria). In contrast, there was no significant difference in the population distribution of these three subtypes in *Gas7*-knockout neurons. However, in the *Gas7*-knockout neurons, subtype 1 was decreased and subtype 6 was increased significantly compared with wild-type neurons (Figure 4C). Similar to the mitochondrial–nuclear boundary mean distance, overexpression of the

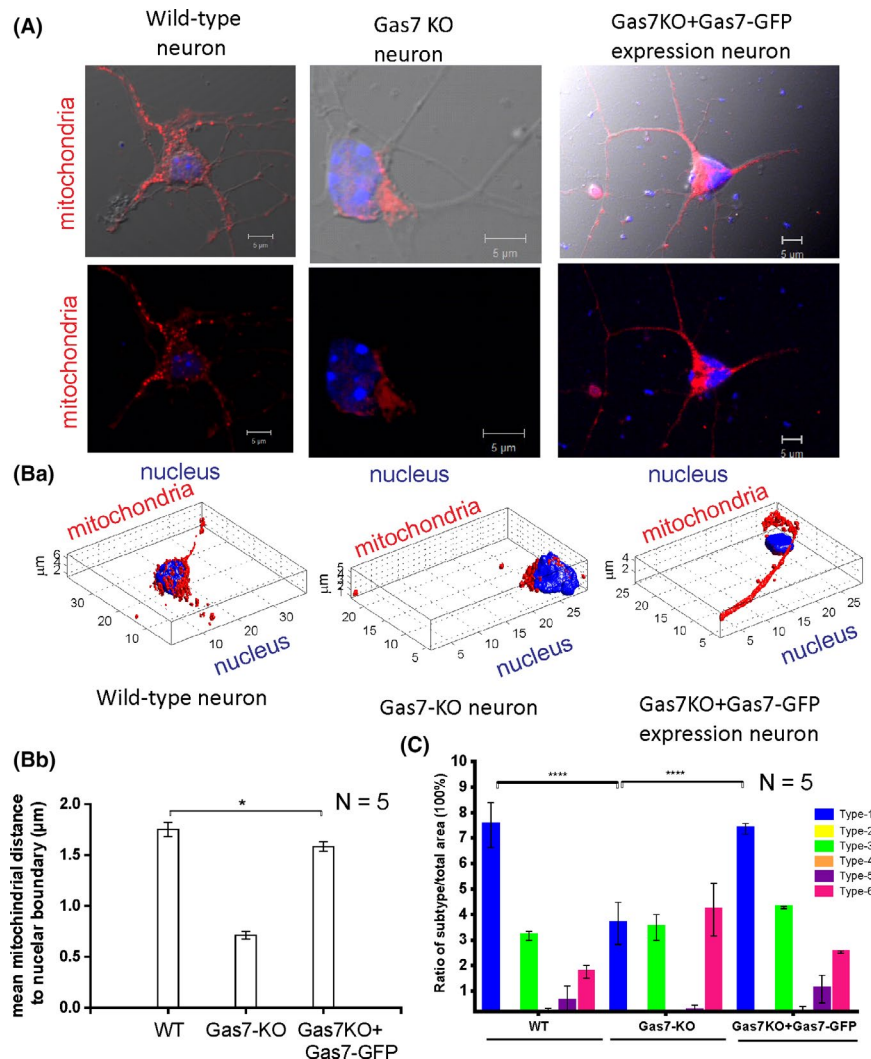


**FIGURE 4** Mitochondrial morphology and heterogeneity is affected in *gas7*-knockout neurons compared with wild-type neurons and can be rescued by ectopic expression of *Gas7*. A, Immunofluorescence analysis of nuclei and mitochondrial staining (labeled red using SDHA antibodies) in wild-type neurons, *gas7*-knockout neurons, and *gas7* KO + *Gas7*-GFP neurons. Top panel shows wild-type neurons, *gas7*-knockout neurons, or *gas7*-knockout neurons rescued with *Gas7* ectopic expression, with mitochondria in red and nucleus in blue shows with merged images of these neurons with DIC images of the respective neurons to show neuronal morphology. Bottom panel shows merged images mitochondria and nucleus of these neurons without DIC images of the respective neurons. Ba, Changes in mitochondrial distribution in wild-type neurons, *gas7*-knockout neurons, or *gas7* KO + *Gas7*-GFP neurons (ie, rescued by *Gas7* ectopic expression) using Micro-P 3D analysis. Immunofluorescence staining of nuclei (blue) and mitochondria (red) indicates the dispersed distribution of mitochondria in wild-type or the perinuclear clustering of mitochondria in *gas7*-knockout neurons. Ectopic expression of *Gas7* can restore the dispersed distribution of mitochondria in *gas7*-knockout neurons. Bb, A presentation of mean distance from mitochondria to the nuclear boundary (μm) calculated using Micro-P 3D software. Bar graphs for wild-type, *gas7*-knockout, and *gas7* KO + *Gas7*-GFP neurons are expressed as means ± SD n = 5, columns = means; error bars = SEs. C, Micro-P classified mitochondria into six types: small fragmented (type 1, blue), large fragmented (type 2, yellow), straight tubular (type 3, green), curved tubular (type 4, orange), horseshoe/donut/network tubular (type 5, purple), or branching tubular (type 6, pink). Bar graph showing the percentages of each type of mitochondria, expressed as means ± SD. n = 5, \*P < .001



Gas7-GFP fusion in *Gas7*-knockout neurons also rescued the distributions of the two mutant subtypes, producing ratios that are similar to the corresponding subtype in wild-type cultures (Figure 4C). Our results indicate that *Gas7*-knockout neurons have differences from wild-type neurons in proportion of mitochondrial subtypes and mitochondrial distribution that can be rescued by ectopic expression of *Gas7*. Therefore, our data suggest that *Gas7* is required for proper mitochondrial morphology and distribution in neurons.

### 3.5 | *Gas7*-knockout mice exhibit imbalanced mitochondrial fusion and fission

Mitochondrial dynamics (fission and fusion) control the shape and distribution of mitochondria in neurons.<sup>25</sup> When fusion predominates, the mitochondria appear as branched filaments, and the organelles become separated particles when fission occurs preferentially.<sup>26</sup> In neurons, filamentous mitochondria are often found in the soma, whereas mitochondria in neurites usually appear as short filaments or spots.<sup>24</sup> Abnormalities in intracellular mitochondrial distribution and morphology in *Gas7*-knockout cortical primary neurons were rescued by the ectopic expression of *Gas7*. Therefore, we hypothesized that mitochondrial fusion and fission might be out of balance in the absence of *Gas7*.

Several widely known ubiquitously expressed proteins are required for mitochondrial fusion and fission. We first determined the expression levels of outer and inner mitochondrial membrane fusion proteins, Mfn-1, Mfn-2, and Opa-1 in the brain lysate of wild-type, heterozygous, and *Gas7*-knockout mice at 60 days of age. In all experiments, GAPDH was used as a protein loading control. Our results show that levels of the outer membrane fusion proteins Mfn-2 and Mfn-1 are increased in heterozygous and KO mice and the increase is significant in *Gas7*-knockout mice (Figure 5A; three samples for each genotype; Mfn-2 and Mfn-1 are, respectively, labeled as Mitofusin-2 and Mitofusin-1). For Mfn-2 and Mfn-1, quantitative data are shown in Figure 5A1,A2, respectively. No significant difference in the protein level of the inner membrane fusion protein Opa-1 was observed (Figure 5A). The increased level of mitochondrial fusion proteins in *Gas7*-knockout brain lysates suggests that mitochondrial fusion may be up-regulated in *Gas7*-knockout mice.

The division of mitochondria is controlled in part by the phosphorylation status of Drp-1 at Serine 616 (targeted by CDK1/cyclin B or CDK5),<sup>27</sup> and at Serine 637 (targeted by protein kinase A, PKA).<sup>28</sup> Mitochondrial fission is inhibited when Drp-1 is phosphorylated at Serine 637, with inactivated Drp-1 distributed to the cytoplasm.<sup>29</sup> Once activated by dephosphorylation at Serine 637, phosphorylation at serine 616 or both, cytosolic Drp-1 translocates to the mitochondrial

outer membrane, where it interacts with one or more of its binding partners, such as fission protein 1 (Fis-1), to initiate mitochondrial fission.<sup>30</sup>

We determined the expression and phosphorylation status of mitochondrial fission protein Drp-1 in mouse brain lysate. As shown in Figure 5B, wild-type, heterozygous and *Gas7*-knockout mice had similar Drp-1 protein levels and Fis-1. However, Drp-1 phosphorylation at Serine 637 was increased and at Serine 616 decreased in both heterozygous and *Gas7*-knockout mice compared with wild types (Figure 5B1,B2). Based on the increase in Drp-1 phosphorylation at Serine 637 in *Gas7*-knockout mice, we anticipated that the activity of the putatively responsible kinase, PKA, is also higher in *Gas7*-knockout mice. Therefore, we investigated PKA activity by determining the status of PKA-dependent phosphorylation of CREB Serine 133<sup>31</sup> in these mice. Our data show that although total CREB protein levels remain similar in these mice (Figure 5B, 14Th panel), phosphorylation of CREB at serine 133 is significantly increased in the heterozygous and *Gas7*-knockout mice (Figure 5B, 12Th panel). Therefore, the data agree with the observed increase in Drp-1 Serine 637 phosphorylation. However, the Drp-1 Serine 166 kinase, CDK5, was not significantly different between these mouse strains (Figure 5B, quantitative data Figure 5B3). As phosphorylation of Serine 166 was decreased, the CDK5 activators, P35 and P25, may have been affected by the absence of *Gas7*.

In summary, our results show that *Gas7*-deficient (heterozygous or knockout) mice had higher levels of mitochondrial fusion proteins Mfn-1 and Mfn-2, decreased phosphorylation of Drp-1 at Serine 616, and increased phosphorylation of Drp-1 at Serine 637. Together the changes in these protein levels would be expected to result in an imbalance in mitochondrial dynamics that would produce an 'over-fused' mitochondrial phenotype in *Gas7*-knockout mice.

### 3.6 | *Gas7*-KO mice have decreased levels of PINK1 and decreased phosphorylation of Parkin (S65), Ubiquitin (S65), and Mitofusion-2 (S442)

Recent studies have suggested that the combination of mitochondrial network dynamics and mitochondrial autophagy (mitophagy) comprise a system of mitochondrial quality control.<sup>32</sup> Mitophagy removes dysfunctional mitochondria, predominantly via a PINK1-Parkin-mediated pathway.<sup>33</sup> Based on our observation of elongated mitochondria and imbalanced mitochondrial dynamics in the absence of *Gas7*, we further measured the levels of key players in mitophagy, such as PINK1, Parkin, phosphorylated Parkin, and ubiquitin,<sup>34,35</sup> in *Gas7*-deficient brain tissue. We found that a significant decrease in protein levels for PINK1 in *Gas7*-deficient brain tissues (Figure 6A, quantitative data

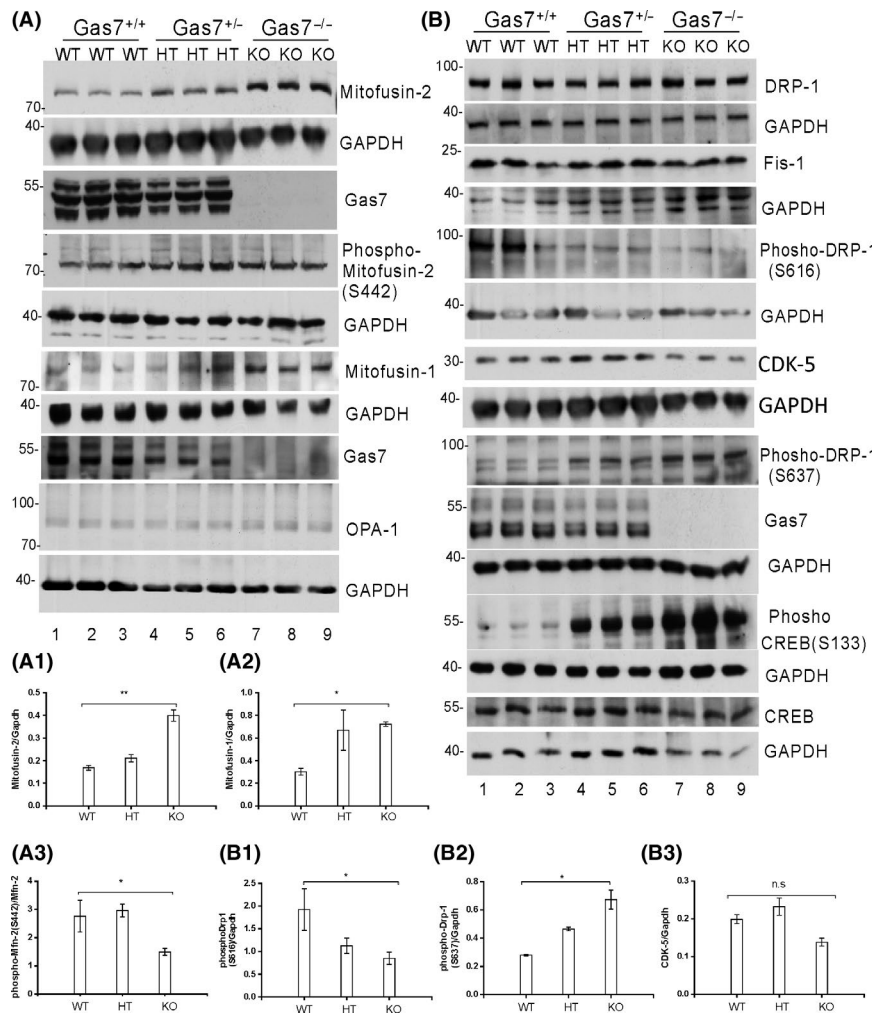


**FIGURE 5** Profusion and profission inhibitor protein levels are increased in *gas7*-knockout mouse cerebrum. A, Western blot analysis. Total brain lysates from wild-type (WT), *gas7* heterozygous (HT), and *gas7*-knockout (KO) mice were electrophoresed by 10% SDS-PAGE. After blotting, the membranes were probed with Gas7 antibody and show that Gas7 protein exists in wild-type and *gas7* heterozygotes but not in *gas7*-knockout mice. Blots detecting Mitofusin-2, phospho-mitofusin-2 (S442), Mitofusin-1, and Opa-1 from cerebrum lysates of *Gas7* WT, HT, and KO mice show increased mitofusin proteins in HT and KO mice compared with WT mice. GAPDH was used as a loading control. A1, Quantification analysis of expression of Mfn-2 protein levels when normalized with GAPDH, showing that Mfn-2 levels increased significantly among WT, *gas7* HT, and *gas7* KO mice. A2, Quantification analysis of expression of Mfn-1 protein levels when normalized with GAPDH showing Mfn-1 levels increased significantly among WT, *gas7* HT, and *gas7* KO mice. A3, Quantification analysis of the phosphorylation status of Mfn-2 protein levels (S442) when normalized with nonphosphorylated Mfn-2 showing that Mfn-2 phosphorylation decreased significantly among WT, *gas7* HT, and *gas7* KO mice. B, Western blot analysis. Total brain lysates from WT, *gas7* HT, and *gas7* KO mice were electrophoresed by 10% SDS-PAGE. After blotting, the membranes were probed with Gas7 antibody to show that Gas7 protein exists in wild-type and *gas7* heterozygotes, but not in *gas7*-knockout mice. Blots to detect expression of Drp-1, GAPDH, Gas7, Fis-1, phospho-Drp-1(S616), phospho-Drp-1(S637), phospho-CREB(S133), CREB, CDK-5, and GAPDH from cerebrum lysates of *Gas7* WT, HT, and KO mice show decreased phospho-Drp-1(S616) (quantified in B2) and increases in both phospho-Drp-1 (S637) (quantified in B1) and phospho-CREB in HT and KO mice compared with WT mice. There were no significant changes in Drp-1, Fis-1, CDK-5 (quantified in B3), or CREB protein levels. GAPDH was used as a loading control

Figure 6A1), with corresponding decreases in PINK1-phosphorylated Parkin (serine 65) and Ubiquitin at serine 65 in *Gas7*-knockout brain tissues (Figure 6A, quantitative data Figure 6A1-6). After ectopic expression of Gas7, mitochondrial fission was increased, with a coincident increase in neurite length and rescue of mitochondrial distribution along the neurite. Thus, Gas7 expression alleviated the perinuclear distribution of elongated mitochondria and

promoted the proper distribution of smaller mitochondria (Figure 4). Ectopic expression of Gas7 also increased PINK1 expression and activation, which likely was responsible for increasing the levels of phosphorylated Parkin protein (Figure S1). This activation of Parkin is expected to facilitate the removal of damaged mitochondria by mitophagy, increasing the proportion of healthy mitochondria to promote neurite outgrowth. Overexpression of wild-type

PINK1 is known to promote neurite outgrowth in SH-SY5Y cells and increase dendritic lengths in primary cortical and midbrain dopaminergic neurons.<sup>36</sup> Gas7 ectopic expression also upregulated miro-1 protein (Figure S1), which is involved in the transport of mitochondria along neurites. Mitochondrial transport is expected to further aid in neurite elongation. Notably, the activity of the Miro proteins is regulated by PINK1 via PKA.<sup>37</sup> Overall, the abnormalities rescued by ectopic expression of Gas7 should help to increase mitochondrial fission and mitochondrial distribution by promoting mitophagy via PINK1-Parkin, which will subsequently promote neurite outgrowth and influences neuronal function. This finding supports our previous known role of Gas7 in regulating neurite outgrowth in Purkinje neurons<sup>7</sup> and hippocampal neurons.<sup>8</sup> We also showed that the absence of Gas7 leads to a decrease in cortical neurite length in *Gas7*-mutant mice.<sup>13</sup>

PINK1 phosphorylation of Mfn-2 at serine 442 mediates Parkin recruitment to damaged mitochondria and serves as a Parkin receptor to stimulate the elimination of damaged mitochondria.<sup>38</sup> Based on the decreased levels of PINK1 and PINK1-phosphorylated Parkin (serine 65), we next measured

phosphorylation of Mfn-2 at serine 442. As shown in Figure 5A, the absence of Gas7 increased Mfn-2 protein levels, but PINK1-phosphorylated Mfn-2 (serine 442) was not drastically increased. Quantitative analysis showed that the relative level of PINK1 phosphorylation of mitofusin-2 (serine 442) was decreased (Figure 5A3). Our results show that a decrease in PINK1 in *Gas7*-knockout mice corresponds to decreases in putative PINK1 phosphorylation of Parkin and Mfn-2.

### 3.7 | *Gas7*-null mice exhibit lower mitochondrial respiration and energy expenditure as well as mitochondrial physiology abnormalities

As we observed an imbalance in mitochondrial dynamics and reduced mitochondrial quality control in cortical tissue of animals without Gas7, we next sought to evaluate whether mitochondrial physiology or function might be affected in *Gas7*-knockout mice. We compared wild types and *Gas7* knockouts at 36 weeks of age, using metabolic chambers to analyze respiration, energy consumption, body mass, and

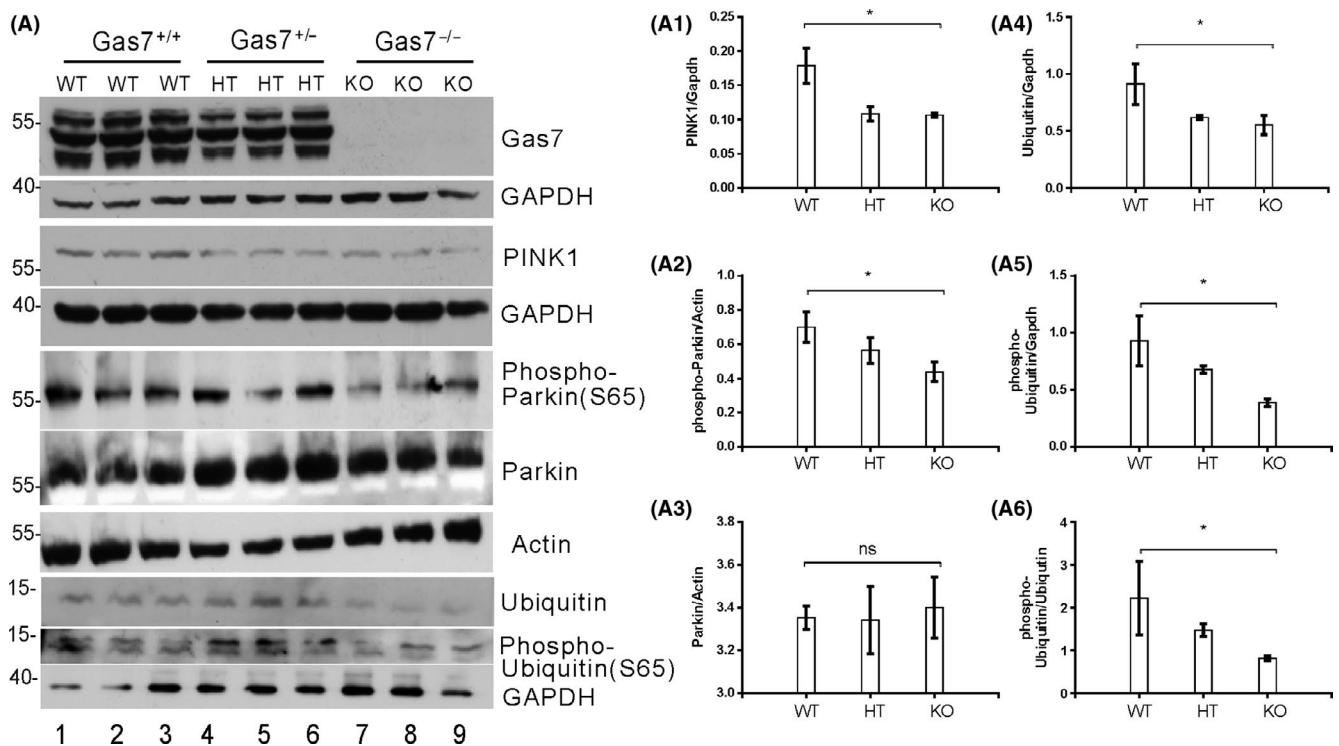


**FIGURE 6** Activation of mitophagy-upstream kinase PINK1, mitophagy proteins, and Parkin is decreased in *gas7*-knockout mouse cerebrum. A, Western blot analysis. Total brain lysates from wild-type (WT), *gas7* heterozygous (HT), and *gas7*-knockout (KO) mice were electrophoresed by 10% SDS-PAGE. After blotting, the membranes were probed with Gas7 antibody to show that Gas7 protein exists in wild-type and *gas7* heterozygotes, but not in *gas7*-knockout mice. Blots show decreased PINK1, phospho-Parkin (S65), Ubiquitin, and phospho-Ubiquitin (S65) proteins in HT/KO mice. There were no significant differences for Parkin protein levels among WT, HT, or KO mice. GAPDH was used as a loading control. Quantification analysis of PINK1 (A1), phospho-Parkin (A2), Ubiquitin (A4), phospho-Ubiquitin (A5), and normalized phospho-Ubiquitin (S65) over normalized Ubiquitin (A6) shows decreases in PINK1, phospho-Parkin, Ubiquitin, and phospho-Ubiquitin in KO mice. Actin and GAPDH were used as loading controls, for which there were no significant differences among WT, HT, or KO mice

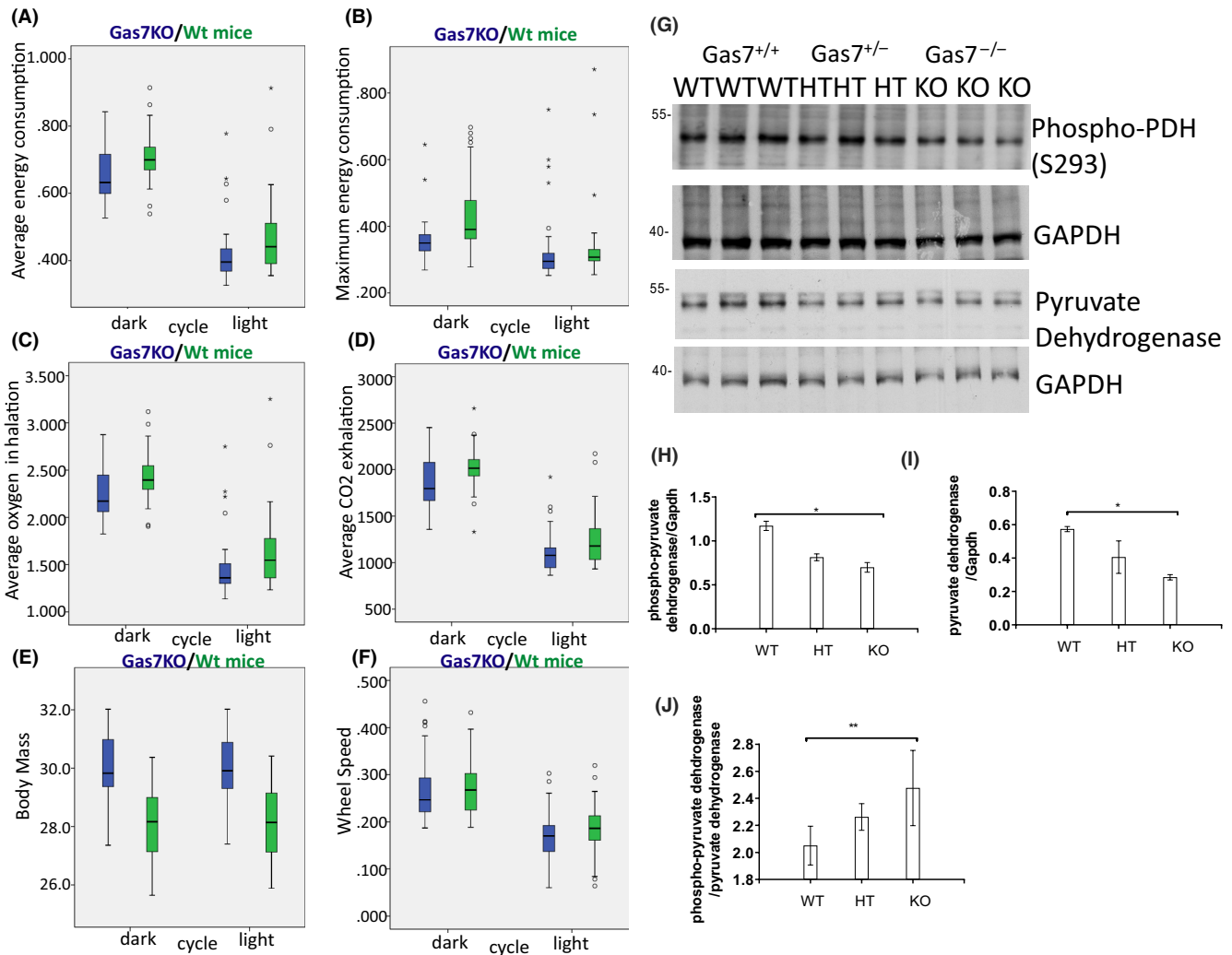


**FIGURE 7** *gas7*-knockout mice exhibit decreased energy consumption, respiration, and wheel speed, as well as increased body mass. A, Box plot analysis of average energy consumption by *Gas7* wild-type (WT, green) and -knockout (KO, blue) male mice, showing decreased average energy consumption of *gas7* KO mice during both the dark (left side) and light (right side) cycles. B, Box plot analysis of maximum energy consumption for *Gas7* WT (green) and KO (blue) male mice, revealing decreased maximum energy consumption of *gas7* KO mice during both dark (left side) and light (right side) cycles. C, Box plot analysis of average oxygen inhalation by *Gas7* WT (green) and KO (blue) male mice, showing decreased average oxygen inhalation of *gas7* KO mice during both the dark (left side) and light (right side) cycles. D, Box plot analysis of differences in average CO<sub>2</sub> exhalation for *Gas7* WT (green) and KO (blue) male mice, demonstrating a decrease in average CO<sub>2</sub> exhalation of *gas7* KO mice during both the dark (left side) and light (right side) cycles. E, Box plot analysis of body mass differences for *Gas7* WT (green) and KO (blue) male mice, showing increased body mass of *gas7* KO mice during both the dark (left side) and light (right side) cycles. F, Box plot analysis of differences in wheel speed for *Gas7* WT (green) and KO (blue) male mice, revealing a decrease in wheel speed of *gas7* KO mice during both the dark (left side) and light (right side) cycles. G, Western blot analysis. Total brain lysates from wild-type (WT), *gas7* heterozygous (HT), and *gas7*-knockout (KO) mice were electrophoresed by 10% SDS-PAGE. After blotting, membranes were probed with phospho-PDH (S293) and pyruvate dehydrogenase (PDH) antibodies. Blots show decreased levels of phospho-PDH and PDH in HT and KO mice. GAPDH was used as a loading control. H, Quantification analysis of phospho-PDH normalized to GAPDH levels, showing the decrease in PDH phosphorylation. I, Quantification analysis of PDH normalized to GAPDH levels, showing the decrease in levels of PDH. J, Quantification analysis of normalized phospho-PDH over normalized PDH levels, showing phosphorylation levels of PDH increase significantly among WT, *gas7* HT, and *gas7* KO mice

muscle strength during light and dark cycles. *Gas7*-knockout animals (blue) exhibited lower average and reduced maximum energy expenditure levels irrespective of dark and light when compared with wild-type mice (Figure 7A,B). The average O<sub>2</sub> inhalation and CO<sub>2</sub> exhalation of *Gas7*-knockout mice was also lower in both light and dark periods (Figure 7C,D).

The lower respiration rates in *Gas7* knockouts suggest that mitochondrial respiration and oxidative phosphorylation might be decreased. We also compared the fitness of mice with the light-dark cycle periods, *Gas7* knockouts had increased body mass compared with wild-type mice (Figure 7E) and decreased running-wheel rotation speed (Figure 7F).

These quantitative data are consistent with the idea that mitochondrial function and physiology might be disrupted in *Gas7*-knockout mice compared with wild type. The irreversible decarboxylation of pyruvate occurs via pyruvate dehydrogenase (PDH) and comprises the entry step into the TCA cycle. Thus, PDH is one of the most important enzymes in the regulation of mitochondrial metabolism. We found that PDH levels were significantly reduced in *Gas7*-knockout brain tissue (Figure 7G,I). Site-specific phosphorylation of serine residues in PDH by different kinases (especially at Serine 293) inhibits protein catalytic activity.<sup>39</sup> We found an increase in this phosphorylation of PDH in both heterozygous and homozygous *Gas7*-knockout mice compared with wild types (Figure 7J). Based on these findings, we conclude that mitochondrial metabolism in the brain is likely to be underutilized in the absence of *Gas7*.

## 4 | DISCUSSION

Mitochondrial function is highly dependent on the morphology and localization of the organelle.<sup>40</sup> Improper organelle size, distribution, and degradation may lead to major deficiencies in mitochondrial functions, such as calcium buffering and energy production.<sup>41</sup> Therefore, mitochondrial morphology and mitophagy are tightly regulated throughout the lifespan of a cell according to its physiological state.<sup>42</sup> Mitochondrial morphology is regulated by mitochondrial fission and fusion dynamics, which are generally mediated by large GTPases, such as Mfn-1, Mfn-2, Opa-1, and Drp-1.<sup>43</sup> Meanwhile, mitophagy is regulated by PINK1 and Parkin signaling.<sup>44</sup> These processes are then coordinated via cell signaling events, such as those mediated by PKA, and crosstalk between signaling pathways.<sup>45</sup> By generating an improved *Gas7*-knockout mouse line, we found that *Gas7* deficiency perturbs these homeostatic processes in neurons at multiple levels, resulting in the accumulation of elongated mitochondria within perinuclear clusters (Figure 8A). This new knockout mouse line is better than previous models in terms of *Gas7* deletion in that it precludes the expression of alternative splicing forms (Figure 1). We inserted a framing error in the *Gas7* gene to create a stop codon in exon 12 to prevent alternative splicing. Thus, these knockout mice are an ideal model system for investigating the in vivo functions of *Gas7*.

Human *GAS7* is a causal gene for obesity based on studies of human *GAS7* transgenic mice.<sup>14</sup> Here, we report that *Gas7*-null mice exhibit lower average energy and reduced maximum energy expenditure levels, increased body weight, and decreased mitochondrial respiration and oxidative phosphorylation, perhaps reflecting a decreased metabolic rate. Together, these findings suggest that mouse *Gas7* acts like a lean gene, consistent with human *GAS7*.

Our study focuses on brain tissues and the results suggest that *Gas7* plays a positive role in sustaining healthy mitochondrial dynamics in neurons. Interestingly, in this study, we have shown that *Gas7* can restore mitochondrial distribution and mitochondrial subtypes in cortical neurons, indicating that *Gas7* can regulate mitochondrial dynamics and contributes to metabolism by acting like a lean gene. Although *Gas7* expression is abundant in brain and testis, the mechanism underlying *Gas7*-mediated regulation of pyruvate dehydrogenase and that enhances the metabolic rates of mice requires further study.

Apart from this metabolic regulation, *Gas7* also regulates CDK5 and PKA kinase activities. As a decrease in the activity of CDK5 and an increase in PKA activity promote mitofusion in the absence of *Gas7* through posttranslational regulation of Drp-1, further decreases in Drp-1 GTPase activity result in mitochondrial elongation and inhibition of fission.<sup>46</sup> Here, we have shown that PKA activity is higher in terms of increased phosphorylation of its well-known target substrate CREB. The mechanism of how *Gas7* regulates PKA and CDK5 activity to promote mitofission remains unknown.

In wild-type neurons, enhanced phosphorylation of Ubiquitin (serine 65) and Parkin (serine 65) is required for degradation of Mitofusin-1/2 by PINK1 and the Parkin-mediated pathway to promote mitofission.<sup>35</sup> In contrast, because of the decrease in PINK1 kinase expression in *gas7*-knockout mice, there is an increase in expression of Mitofusin-1/2 that enhances mitofusion and results in defects of mitochondrial distribution and perinuclear clustering. The ubiquitination of mitofusins may be reduced in the absence of *Gas7*, ultimately promoting mitofusion (Figure 8A). *Gas7* can rescue levels of PINK1 protein expression in cortical neurons and restore its activity by increasing phosphorylation of its substrate Parkin (S65) (Figure S1), suggesting that *Gas7* regulates mitochondrial dynamics specifically in neurons and brain tissue. Collectively, our data indicate that *Gas7* is required for the regulation of PINK1, Parkin, and phospho-Parkin proteins which control mitophagy, so mitophagy initiation may be inhibited in the brains of *gas7*-knockout mice due to enhanced mitofusion and perinuclear clustering.

Pyruvate dehydrogenase complex (PDC) plays a major role in regulating mammalian metabolism by utilizing carbohydrate, thereby helping to maintain glucose homeostasis and contributing to the metabolic pathways required for energy production and movement.<sup>47-49</sup> Recent studies provided a link between diet-dependent modulation of mitochondrial fusion in specific neurons and whole-body energy metabolism of the animal.<sup>50</sup> From this study, they suggest that overfeeding leads to mitochondria elongation by Mfn1/2-dependent manner in hypothalamic neurons.<sup>51</sup> These studies open new avenues of research to understand how mitochondrial dynamics changes in the hypothalamus

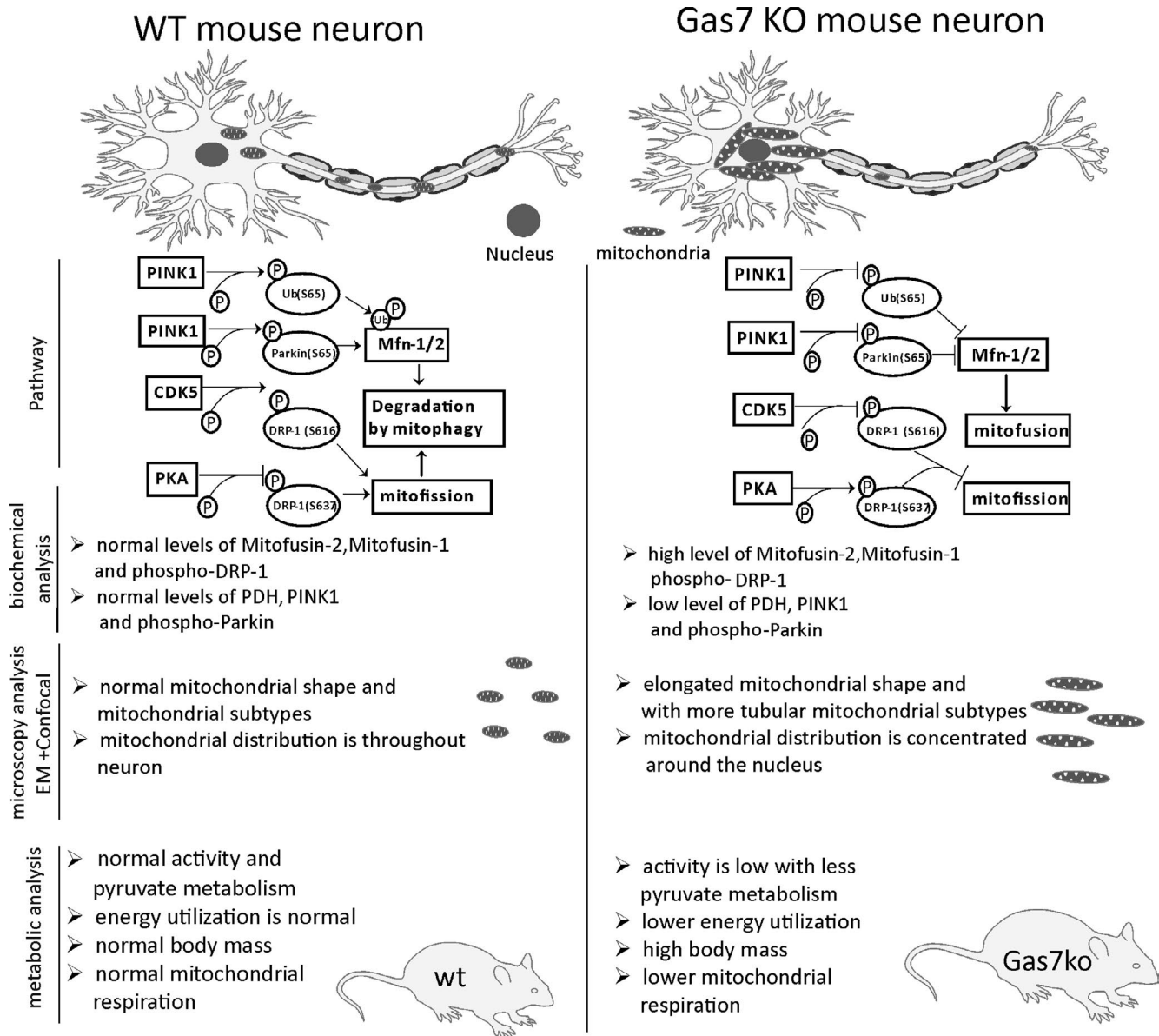


**FIGURE 8** Comparison between wild-type and *gas7*-knockout neurons of mitofusin regulation by the PINK1 and parkin-mediated mitophagy pathway. Comparison of the mitochondrial distribution between wild-type and *gas7*-knockout neurons and differences in the regulatory pathway, as well as summarized results of biochemical analyses, differences in mitochondrial morphology as observed by microscopy, and metabolic differences for wild-type and *gas7*-knockout mice

affect distal metabolic organs. Similarly we observed elongated mitochondria in cortical tissue and we have shown that energy consumption and muscle strength are diminished in *Gas7*-knockout mice, indicating that maybe mitochondrial dynamics and function in muscles are not optimal. We also detected decreased expression and activity of pyruvate dehydrogenase (PDH) in *Gas7*-knockout mice, it will be interesting to know how mitochondrial dynamic changes in cortex affect metabolic enzyme PDH expression. We did not observe any significant differences in PDH mRNA levels or for the kinases responsible for PDH inactivation in wild-type and *Gas7*-knockout mice (data not shown), and reexpression of *Gas7* alone could not

rescue the reduced expression of PDH in *gas7*-knockout neurons (Figure S1). This decreased expression of PDH indicates that ATP generation may be inhibited because the conversion of acetyl-co-A by pyruvate is reduced. This decrease in pyruvate metabolism results in reduced muscle strength and muscle contraction, mirroring the symptoms of PD patients. We have shown that *gas7*-knockout mice have lower energy consumption and decreased wheel rotation speed compared with wild-type (Figure 7A-F), suggesting that reduced Parkin activity is responsible for the muscle strength weakness they display. Accordingly, it would be interesting to establish the relationship between *Gas7* and parkin proteins. Metabolic disorders arising from

deficiencies of the PDH/PDK system manifest as defects in the synthesis, metabolism, transportation, and storage of biochemical compounds. Further study is required to investigate the regulation of pyruvate metabolites in the absence of Gas7. We also observed decreased protein expression of Tyrosine Hydroxylase (TH) in *gas7*-knockout mouse cerebrum lysates (data not shown), indicating that Gas7 may affect the functioning of dopaminergic neurons and the synthesis of dopamine. Therefore, Gas7 may regulate motor function through its effect on mitochondria in dopaminergic neurons, which warrants further study. Moreover, our previous study showed that aged *gas7*-deficient mice exhibit abnormal muscle fiber composition, reduced nerve terminal sprouting of neuromuscular junctions, and reduced motor function.<sup>13</sup> Thus, Gas7 may be involved in motor function through various types of neurons and we will address some of the potential mechanisms in future studies.

In summary, our results suggest a mechanism by which Gas7 acts as a positive molecular mediator of mitochondrial dynamics and mitophagy, thereby sustaining a healthy mitochondrial population in neurons.

#### ACKNOWLEDGEMENTS

The *gas7*-knockout mice were created by the Transgenic Mouse Model Core Facility of the National Core Facility Program for Biotechnology, Ministry of Science and Technology, Taiwan, and the Gene Knockout Mouse Core Laboratory of National Taiwan University Center for Genomic Medicine. SNP genotyping was performed by the National Center for Genome Medicine, located at the Institute of Biomedical Sciences, Academia Sinica. We also thank Dr J. O'Brien for manuscript editing services. This work was supported by an intramural fund from the Institute of Molecular Biology, Academia Sinica, and a theme project of Academia Sinica (2323). This work fulfilled in part the requirements for the PhD thesis of JNB, Molecular Cell Biology, Taiwan International Graduate Program, Institute of Molecular Biology, Academia Sinica and Graduate Institute of Life Sciences, National Defense Medical Center, Taipei, Taiwan. We would like to thank National RNAi Core Facility, Academia Sinica, Taiwan.

#### CONFLICT OF INTEREST

The authors state that there are no actual or potential conflicts of interest.

#### AUTHOR CONTRIBUTIONS

JNB and SLC conceived and designed the experiments, analyzed the data, and wrote the paper; JNB performed experiments for Figures 2, 4-8 and Figure S1, BTH performed experiments for Figure 1, and GGL performed the experiment for Figure 3. MJC contributed intellectually to the final version of the manuscript.

#### REFERENCES

- Brenner DG, Lin-Chao S, Cohen SN. Analysis of mammalian cell genetic regulation in situ by using retrovirus-derived "portable exons" carrying the *Escherichia coli lacZ* gene. *Proc Natl Acad Sci USA*. 1989;86:5517-5521.
- Lazakovitch EM, She BR, Lien CL, Woo WM, Ju YT, Lin-Chao S. The *Gas7* gene encodes two protein isoforms differentially expressed within the brain. *Genomics*. 1999;61:298-306.
- Aspenstrom P, Fransson A, Richnau N. Pombe *Cdc15* homology proteins: regulators of membrane dynamics and the actin cytoskeleton. *Trends Biochem Sci*. 2006;31:670-679.
- Ahmed S, Bu W, Lee RT, Maurer-Stroh S, Goh WI. F-BAR domain proteins: Families and function. *Commun Integr Biol*. 2010;3:116-121.
- Su WB, You J-J, Huang B-T, Sivakumar V, Yeh S-D, Lin-Chao S. *The Pombe Cdc15 Homology Proteins*, Madame Curie Bioscience Database. Austin, TX: Landes Bioscience; 2009.
- She BR, Liou GG, Lin-Chao S. Association of the growth-arrest-specific protein *Gas7* with F-actin induces reorganization of microfilaments and promotes membrane outgrowth. *Exp Cell Res*. 2002;273:34-44.
- Ju YT, Chang AC, She BR, et al. *gas7*: A gene expressed preferentially in growth-arrested fibroblasts and terminally differentiated Purkinje neurons affects neurite formation. *Proc Natl Acad Sci USA*. 1998;95:11423-11428.
- You JJ, Lin-Chao S. *Gas7* functions with N-WASP to regulate the neurite outgrowth of hippocampal neurons. *J Biol Chem*. 2010;285:11652-11666.
- Chao CC, Chang PY, Lu HH. Human *Gas7* isoforms homologous to mouse transcripts differentially induce neurite outgrowth. *J Neurosci Res*. 2005;81:153-162.
- Akiyama H, Gotoh A, Shin RW, et al. A novel role for h*Gas7b* in microtubular maintenance: possible implication in tau-associated pathology in Alzheimer disease. *J Biol Chem*. 2009;284:32695-32699.
- Uchida T, Akiyama H, Sakamoto W, et al. Direct optical microscopic observation of the microtubule polymerization intermediate sheet structure in the presence of *gas7*. *J Mol Biol*. 2009;391:849-857.
- Hidaka M, Koga T, Gotoh A, Sanada M, Hirose K, Uchida T. Alzheimer's disease-related protein h*Gas7b* interferes with kinesin motility. *J Biochem*. 2012;151:593-598.
- Huang BT, Chang PY, Su CH, Chao CC, Lin-Chao S. *Gas7*-deficient mouse reveals roles in motor function and muscle fiber composition during aging. *PLoS ONE*. 2012;7:e37702.
- Yang X, Deignan JL, Qi H, et al. Validation of candidate causal genes for obesity that affect shared metabolic pathways and networks. *Nat Genet*. 2009;41:415-423.
- Schadt EE, Lamb J, Yang X, et al. An integrative genomics approach to infer causal associations between gene expression and disease. *Nat Genet*. 2005;37:710-717.
- Scacheri PC, Crabtree JS, Novotny EA, et al. Bidirectional transcriptional activity of PGK-neomycin and unexpected embryonic lethality in heterozygote chimeric knockout mice. *Genesis*. 2001;30:259-263.
- Masu Y, Wolf E, Holtmann B, Sendtner M, Brem G, Thoenen H. Disruption of the *CNTF* gene results in motor neuron degeneration. *Nature*. 1993;365:27-32.

18. Soriano P, Montgomery C, Geske R, Bradley A. Targeted disruption of the c-src proto-oncogene leads to osteopetrosis in mice. *Cell*. 1991;64:693-702.
19. Melanson EL, Ingebrigtsen JP, Bergouignan A, Ohkawara K, Kohrt WM, Lighton JR. A new approach for flow-through respirometry measurements in humans. *Am J Physiol Regul Integr Comp Physiol*. 2010;298:R1571-R1579.
20. Kaiyala KJ, Wisse BE, Lighton JRB. Validation of an equation for energy expenditure that does not require the respiratory quotient. *PLoS ONE*. 2019;14:e0211585.
21. Abreu-Vieira G, Xiao C, Gavrilova O, Reitman ML. Integration of body temperature into the analysis of energy expenditure in the mouse. *Mol Metab*. 2015;4:461-470.
22. Peng JY, Lin CC, Chen YJ, et al. Automatic morphological subtyping reveals new roles of caspases in mitochondrial dynamics. *PLoS Comput Biol*. 2011;7:e1002212.
23. Westermann B. Mitochondrial fusion and fission in cell life and death. *Nat Rev Mol Cell Biol*. 2010;11:872-884.
24. Misgeld T, Schwarz TL. Mitostasis in neurons: maintaining mitochondria in an extended cellular architecture. *Neuron*. 2017;96:651-666.
25. Chen H, Chan DC. Mitochondrial dynamics in mammals. *Curr Top Dev Biol*. 2004;59:119-144.
26. Youle RJ, van der Bliek AM. Mitochondrial fission, fusion, and stress. *Science*. 2012;337:1062-1065.
27. Strack S, Wilson TJ, Cribbs JT. Cyclin-dependent kinases regulate splice-specific targeting of dynamin-related protein 1 to microtubules. *J Cell Biol*. 2013;201:1037-1051.
28. Knott AB, Perkins G, Schwarzenbacher R, Bossy-Wetzel E. Mitochondrial fragmentation in neurodegeneration. *Nat Rev Neurosci*. 2008;9:505-518.
29. Otera H, Wang C, Cleland MM, et al. Mff is an essential factor for mitochondrial recruitment of Drp1 during mitochondrial fission in mammalian cells. *J Cell Biol*. 2010;191:1141-1158.
30. Palmer CS, Elgass KD, Parton RG, Osellame LD, Stojanovski D, Ryan MT. Adaptor proteins MiD49 and MiD51 can act independently of Mff and Fis1 in Drp1 recruitment and are specific for mitochondrial fission. *J Biol Chem*. 2013;288:27584-27593.
31. Montminy MR, Bilezikjian LM. Binding of a nuclear protein to the cyclic-AMP response element of the somatostatin gene. *Nature*. 1987;328:175-178.
32. Youle RJ, Narendra DP. Mechanisms of mitophagy. *Nat Rev Mol Cell Biol*. 2011;12:9-14.
33. Shirihaï OS, Song M, Dorn GW, 2nd. How mitochondrial dynamism orchestrates mitophagy. *Circ Res*. 2015;116:1835-1849.
34. Lutz AK, Exner N, Fett ME, et al. Loss of parkin or PINK1 function increases Drp1-dependent mitochondrial fragmentation. *J Biol Chem*. 2009;284:22938-22951.
35. Durcan TM, Fon EA. The three 'P's of mitophagy: PARKIN, PINK1, and post-translational modifications. *Genes Dev*. 2015;29:989-999.
36. Dagda RK, Pien I, Wang R, et al. Beyond the mitochondrion: cytosolic PINK1 remodels dendrites through protein kinase A. *J Neurochem*. 2014;128:864-877.
37. Das Banerjee T, Dagda RY, Dagda M, et al. PINK1 regulates mitochondrial trafficking in dendrites of cortical neurons through mitochondrial PKA. *J Neurochem*. 2017;142:545-559.
38. Chen Y, Dorn GW, 2nd. PINK1-phosphorylated Mitofusin 2 is a Parkin receptor for culling damaged mitochondria. *Science*. 2013;340:471-475.
39. Holness MJ, Sugden MC. Regulation of pyruvate dehydrogenase complex activity by reversible phosphorylation. *Biochem Soc Trans*. 2003;31:1143-1151.
40. Chen H, Chan DC. Mitochondrial dynamics—fusion, fission, movement, and mitophagy—in neurodegenerative diseases. *Hum Mol Genet*. 2009;18:R169-R176.
41. Melder S, Lavie J, Benard G. Mitochondrial degradation and energy metabolism. *Biochem Biophys Acta*. 2015;1853:2812-2821.
42. Rambold AS, Lippincott-Schwartz J. Mechanisms of mitochondria and autophagy crosstalk. *Cell Cycle*. 2011;10:4032-4038.
43. Wai T, Langer T. Mitochondrial dynamics and metabolic regulation. *Trends Endocrinol Metab*. 2016;27:105-117.
44. Jin SM, Youle RJ. PINK1- and Parkin-mediated mitophagy at a glance. *J Cell Sci*. 2012;125:795-799.
45. Ould Amer Y, Hebert-Chatelain E. Mitochondrial cAMP-PKA signaling: What do we really know? *Biochim Biophys Acta Bioenerg*. 2018;1859:868-877.
46. Taguchi N, Ishihara N, Jofuku A, Oka T, Mihara K. Mitotic phosphorylation of dynamin-related GTPase Drp1 participates in mitochondrial fission. *J Biol Chem*. 2007;282:11521-11529.
47. Dunford EC, Herbst EA, Jeoung NH, et al. PDH activation during in vitro muscle contractions in PDH kinase 2 knockout mice: effect of PDH kinase 1 compensation. *Am J Physiol Regul Integr Comp Physiol*. 2011;300:R1487-R1493.
48. Denton RM, Halestrap AP. Regulation of pyruvate metabolism in mammalian tissues. *Essays Biochem*. 1979;15:37-77.
49. Peters SJ, St Amand TA, Howlett RA, Heigenhauser GJ, Spriet LL. Human skeletal muscle pyruvate dehydrogenase kinase activity increases after a low-carbohydrate diet. *Am J Physiol*. 1998;275:E980-E986.
50. Dietrich MO, Liu ZW, Horvath TL. Mitochondrial dynamics controlled by mitofusins regulate Agrp neuronal activity and diet-induced obesity. *Cell*. 2013;155:188-199.
51. Schneeberger M, Dietrich MO, Sebastian D, et al. Mitofusin 2 in POMC neurons connects ER stress with leptin resistance and energy imbalance. *Cell*. 2013;155:172-187.

## SUPPORTING INFORMATION

Additional supporting information may be found online in the Supporting Information section.

**How to cite this article:** Bhupana JN, Huang B-T, Liou G-G, Calkins MJ, Lin-Chao S. Gas7 knockout affects PINK1 expression and mitochondrial dynamics in mouse cortical neurons. *FASEB BioAdvances*. 2020;2:166–181. <https://doi.org/10.1096/fba.2019-00091>